ASME Journal of Tribology
Online journal at:
https://asmedigitalcollection.asme.org/tribology

Henry Ing
Department of Bioengineering,
University of Pittsburgh,
3700 O'Hara St., Benedum Hall Room 302,
Pittsburgh, PA 15261
e-mail: henrying12@gmail.com

Vimanyu Chadha
Department of Mechanical Engineering and
Materials Science,
University of Pittsburgh,
3700 O'Hara St., Benedum Hall Room 636,
Pittsburgh, PA 15261
e-mail: vic55@pitt.edu

Anna B. Randolph
Department of Bioengineering,
University of Pittsburgh,
3700 O'Hara St., Benedum Hall Room 302,
Pittsburgh, PA 15261
e-mail: abr56@pitt.edu,

Ky Reifler
Department of Mechanical Engineering and
Materials Science,
University of Pittsburgh,
3700 O'Hara St., Benedum Hall Room 636,
Pittsburgh, PA 15261
e-mail: reiflerhama@earthlink.net

Tevis D.B. Jacobs
Department of Mechanical Engineering and
Materials Science,
University of Pittsburgh,
3700 O'Hara St., Benedum Hall Room 636,
Pittsburgh, PA 15261
e-mail: tjacobs@pitt.edu

Kurt E. Beschorner[1]
Department of Bioengineering,
University of Pittsburgh,
3700 O'Hara St., Benedum Hall Room 302,
Pittsburgh, PA 15261;
Department of Mechanical Engineering and
Materials Science,
University of Pittsburgh,
3700 O'Hara St., Benedum Hall Room 636,
Pittsburgh, PA 15261
e-mail: beschorn@pitt.edu

Validation of a Multiscale Hysteresis Mechanics Model in Predicting Oily Shoe-Floor Friction Across Surfaces With Varying Finishes

Shoe-floor friction, quantified by the coefficient of friction (COF), is an important predictor of the risk of slip-and-fall accidents. There is a commonly used model of friction by B. Persson that describes viscoelastic dissipation due to hysteretic properties of rubber. Applied to shoe-floor friction, the model calculates the COF by using two primary inputs: (1) the multiscale surface topography of floor tiles and (2) the time-dependent material properties of the shoe rubber. While this theory is well accepted by many theoreticians and modelers, there is almost no direct experimental validation. Here, the model is tested by comparing against experimental measurements of COF using three different designs of shoes, ten different porcelain-tile floors, and canola oil as a contaminant. The results demonstrated that, while the model was predictive of trends, its values were too large by an average of 1050% when all scales of topography were included. However, this predictive power was improved ($p < .0001$, $RMS_{error} = 0.066$) when the range of size scales of topography was limited to exclude the smallest-scale topography features. Scientifically, these findings provide new insights about which length scales of topography are most relevant to performance under different conditions. For real-world application, these results show the potential of this model to be used by floor designers and engineers to develop or select materials to create slip-resistant shoes and flooring. This would then create safer workplace environments, decreasing the significant economic burden and human suffering caused by slip-and-fall accidents. [DOI: 10.1115/1.4068109]

Keywords: slips, trips, and falls, shoe-floor friction, viscoelastic hysteresis modeling, surface topography and roughness, bio-tribology, surface roughness and asperities, tires

1 Introduction

Slips, trips, and falls are a serious occupational hazard that are a common source of workplace injuries. About 20% [1] of non-fatal and 16% [2] of fatal occupational injuries occur because of falling incidents. Slipping has been shown to precede 55% of falls on the

[1]Corresponding author.
Contributed by the Tribology Division of ASME for publication in the JOURNAL OF TRIBOLOGY. Manuscript received December 3, 2024; final manuscript received March 3, 2025; published online April 3, 2025. Assoc. Editor: Pradeep Menezes.

same level and 23% of falls to lower levels [3]. Beyond the pain, suffering, and sustained injuries that reduce quality of life, these accidents also come with large financial burdens on those affected and their employers. According to the 2023 Liberty Mutual Workplace Safety Index, the direct cost to employers for medical expenses and lost wages of same-level slips, trips, and falls was estimated to be $10.9 billion [4].

The coefficient of friction (COF) between a shoe and floor in contact has long been recognized as a critical factor affecting the risk of slipping [3,5–8]. This risk is determined by the required COF and the available COF. The required COF is the lowest value necessary for a person to walk without slipping [5,9,10]. This value is determined by gait biomechanics and can be measured by testing ground-reaction forces while walking without slipping (typically about 0.2 for straight walking on level ground) [10]. The available COF describes the friction interaction between a specific shoe and floor, and depends on both biomechanical factors such as normal force and sliding velocity [11,12], as well as characteristics of shoes and floors [13–15]. The available COF is typically measured by tribometers that measure the forces during sliding between samples of shoes and flooring, ideally while simulating the salient biomechanical parameters of slipping such as normal forces, shoe-floor angle and sliding speed [16,17]. As the difference between available and required COF decreases, the risk of slipping increases [5,9,10]. Various studies within workplace environments that have increased the available COF by altering shoe or floor characteristics have shown decreased rates of slipping [18–21].

Shoe-floor friction is caused by multiple mechanisms that occur between the viscoelastic material of the shoe's outsole and the topography of the floor surface. During walking, the surface asperities from the floor interact with the shoe material. The topography that is inherent in any surface leads to incomplete contact between the surfaces, and to variable contact pressures across the floor surface. Thus, this topography can influence friction by altering the real surface area in contact. Friction can also be affected by the energy absorption of the shoe material that occurs during load cycling of the rubber elastomer due to the surface topography [8,22–26]. The friction between the rigid surface and viscoelastic material is commonly attributed to two sources: adhesion—resulting from forces needed to break intermolecular attractions between contacting surfaces—and viscoelastic hysteresis—resulting from energy dissipation due to deformation of viscoelastic materials [22,23,26,27]. Prior research has suggested that adhesion friction is sensitive to the fluids present in boundary lubrication because the presence of fluid (especially polar fluids with long molecular length), interferes with adhesion forces [26,28,29]. However, the hysteresis component of friction is more robust to the presence of fluids [25,26,30]. Thus, adhesion friction may be the dominant factor for dry friction, while hysteresis friction may be the dominant factor for wet or oily friction. The present study focuses on predicting hysteresis friction given this expectation that it dominates oily-floor friction, a condition that is likely to lead to slipping.

Surface topography is the defining characteristic of floors that contributes to friction [22,27,31–36]. Surface topography is most commonly characterized using standard techniques and ISO parameters, such as the average roughness R_a as measured using a stylus profilometer. However, research by the present authors [32] and many other groups [14,34] show only modest correlations between conventional roughness parameters and friction. One possible reason for this limited predictive power is the multiscale nature of surface topography on natural and engineered surfaces. Whereas traditional roughness parameters contain information about only a single size scale of topography, the physical interactions that govern friction likely depend on topography at multiple different length scales [37]. Therefore, it has been proposed that superior predictive power can be achieved using mechanics models that consider multiple scales of topography, as opposed to statistical models based on conventional parameters, which focus primarily on a single size scale [38].

Viscoelastic shoe materials have time-dependent responses to the cyclic loading from the floor asperities during sliding. These responses are dependent on the loading frequency ω, which for a sliding contact is a function of sliding velocity $\bar{v}$ and the wavelength λ of the floor asperity over which it is sliding according to $\lambda = 2\pi\bar{v}/\omega$. This is further controlled by the time-dependent mechanical properties of the shoe material, specifically the complex modulus E:

$$E(\omega) = E'(\omega) + iE''(\omega) \tag{1}$$

which contains both a real component, the storage or elastic modulus E', and an imaginary component, the loss or viscous modulus E'' as indicated in Eq. (1) [23,25,39].

Dynamic mechanical analysis is used to measure the complex modulus across frequencies by shearing a material sample at varying frequencies and temperatures while the force response is measured. To test loading frequencies higher than the device's capacity, time-temperature superposition is typically used [40]. The effects of high-frequency material response on friction, associated with the small-size-scale topography, can be measured by lowering the temperature [23,41,42].

Viscoelastic hysteresis friction is modeled by describing the energy loss from the multi-length-scale topography activating the multi-time-scale response of the shoe material. One such model was developed by Persson, and uses a spectral description of the floor surface (its power spectral density, (PSD)) combined with a spectral description of the elastomer's material response (measured by dynamic mechanical analysis, (DMA)) [25]. The Persson contact models were originally conceived for highly idealized self-affine surfaces; however, the non-adhesive form of the model potentially applies to the non-self-affine topography that is found on many natural and engineered surfaces [43,44]. While the viscoelastic-friction model has not been extensively tested, it is reasonable to assume that it will also generalize beyond idealized topography.

This model also accounts explicitly for non-conformal contact, acknowledging that contact between a shoe and rough surface is "patchy" rather than continuous. The model considers the ratio of the *real* contact area to the *apparent* contact area, since friction is not generated in the non-contact regions. This model also considers the three-dimensional nature of asperities and its impact on the frequency of the induced stresses on the shoe. Furthermore, the Persson model deviates from other contact models [45,46], and shoe-floor friction models that utilize finite element analysis [47], because it does not require commercial software and generally requires less computation time. Finally, the model by Persson was selected over a similar model by Heinrich et al. [48] since the Persson model explicitly considers the scale-dependence of the ratio of real-to-apparent contact area, which other models do not. However, despite the wide use of the Persson model, its experimental validation for use in shoe-floor friction is minimal, with only one prior investigation to-date, which used a very limited set of materials (three shoes and two floors) [49].

Because of the multiscale nature of this model, the present investigation characterized topography over a wide range of size scales. This was accomplished by pairing stylus profilometry, which excels in characterizing features with a wavelength of approximately 10 μm up to 1 mm, with a novel method developed by the present team [32,35,36,50] which uses scanning electron microscopy (SEM) to measure topography down to scales of approximately 10 nm. SEM can be combined with stylus profilometry to characterize topography contributions from a wide range of size scales, thus spanning from 10 nm to 1 mm [50]. As mentioned, the power spectral density provides a spectral description of surface topography across size scales [32,35,36]. Customarily, PSD curves tend to report the topographical power over wavevector q, which is inversely related to wavelength $\lambda = 2\pi/q$.

This study offers a key innovation over prior shoe-floor friction modeling work by accounting for the wide range of scales that are scientifically predicted to control friction: both a wide range

of length-scales in topography, and a correspondingly large range of frequency scales of the frequency-dependent viscoelastic mechanical properties. Thus, this investigation is the first to systematically include friction contributions from all size scales, including submicron wavelengths. The purpose of this study is to assess the ability of a mechanics model based on viscoelastic hysteresis friction to predict oily friction using the multiscale surface topography of flooring and time-dependent material properties of shoes. The model is validated across three shoes and a wide range of porcelain flooring.

2 Methods

2.1 Hysteresis Model. The coefficient of friction is computed as an integral, Eqs. (2)–(4), that takes into account both the wavevector q and the angle ϕ between the sliding direction and any given contribution to topography [25]:

$$\mathrm{COF} = \frac{1}{2}\int_{q_L}^{q_1} q^3 C(q) P(q) \left[\int_0^{2\pi} cos\phi \frac{E''(q\bar{v}cos\phi)}{(1-\nu^2)\sigma_0} d\phi\right] dq \tag{2}$$

$$P(q) = \frac{2}{\pi}\int_0 \frac{\sin x}{x} exp[-x^2 G(q)]\, dx \tag{3}$$

$$G(q) = \frac{1}{8}\int_{q_L}^{q} q^3 C(q) \left[\int_0^{2\pi} \left|\frac{E(q\bar{v}cos\phi)}{(1-\nu^2)\sigma_0}\right|^2 d\phi\right] dq \tag{4}$$

where other variables are defined as follows. The inputs to the model include the power spectral density $C(q)$, the Poisson ratio ν, the sliding velocity $\bar{v}$, and the normal pressure σ_0. While the material modulus is typically specified as E(w), here it is specified as a function of $q\bar{v}cos\phi$ in this model which is equivalent to $\omega cos\phi$ using the previously stated relationship between frequency and wavevector. The inclusion of ϕ allows for 3D topography effects as the material responds differently when moving parallel or perpendicular to a sinusoidal surface. The limits of integration for wavevectors range from q_L to q_1. These correspond to asperities of the largest wavelength ($\lambda_L = 2\pi/q_L$) to the smallest wavelength ($\lambda_1 = 2\pi/q_1$). $P(q)$ is the ratio of apparent area of contact, $A(\lambda)$, to nominal area of contact, $A(L)$. The apparent area of contact at any given size scale comprises the real area of contact with surface asperities of a certain wavelength, while ignoring all smaller wavelength asperities. The nominal area of contact is the macroscopic area of contact ignoring any asperities that may not be in contact. The inclusion of $P(q)$ allows for the COF prediction to account for the fact that the fractional area of contact will vary depending on the size scale that is being considered. The term $P(q)$ is calculated as a function of a coefficient $G(q)$ integrated across the position x in the direction of sliding. The term $G(q)$ serves mainly to incorporate variables such as topography, material properties, speed, and pressure into the area-of-contact calculations.

The COF for all shoe-floor combinations was computed using Persson's model [25]. We note that there are two implementations of this theory: an exact solution (Eq. (30) of [25]), where the integrations are solved numerically, over the measured values of PSD; and an approximate solution (Eq. (36) of [25]), where the PSD is assumed to be linear with a slope related to the Hurst exponent H; the latter facilitates analytical solutions. However, here we use the exact solution, accounting for all topography scales and allowing for non-ideal non-self-affine topography. Specifically, the term $G(q)$ is calculated at each wavevector using the limits of integration from q_L to the current wavevector q, as determined by the limits of integration from the original COF equation (Eq. (2)). This resulting value is then used to calculate $P(q)$. Finally, the actual COF prediction value can be determined by integrating the resulting $P(q)$, PSD, and loss modulus across the full range of wavevector values.

2.1.1 Verification. Numerical integration techniques were used to implement the model. A trapezoidal integration was used to calculate each integral in the equations for $G(q)$ and μ, Eq. (5).

$$\int_{x_0}^{x_n} f(x)dx = \sum_{i=1}^{n-1} \frac{1}{2}[f(x_{i+1}) + f(x_i)][x_{i+1} - x_i] \tag{5}$$

The number of points used n (inversely related to the point density) used for each trapezoidal integration were found using a point-density analysis. Inspired by a mesh-density analysis used in finite element analysis [51], the resulting COF calculations (using inputs discussed in Sec. 2.2.4) from the model were plotted against the number of points used between the limits of integration. The number of points was proportional to the time to run the code; thus, the optimal point density balanced the accuracy and solution time. This optimal density corresponded to the point at which the percent difference between that COF calculation and the COF of the previous point on the curve was less than 1%. A varying number of points ranging from 10 to 10,000 for q was used to calculate the COF of one shoe and floor combination (Shoe A and Floor 1). Only one shoe-floor combination was used because it was assumed that the point densities would have the same effects on COF calculations between all shoes and floors. This analysis was performed for both trapezoidal integration variables, q and ϕ, although the range of number of points for ϕ was 40 to 100 because of the smaller magnitudes of the limits of integration. The optimal densities were found to be 150 points for the q variable and 50 points for the ϕ variable.

The use of the model in this work was verified [52] against simulation results presented by Persson et al. [25]. We replicated the inputs from Persson et al. and compared plots of our simulation results to the published results [25]. The model was considered verified and used in this study after this consistency with prior research was confirmed.

2.2 Experimental Validation. The model was validated by comparing the model COF predictions to experimentally measured COF values. For this process, 3 shoes and 10 floors were used. The shoes (SRMax Atlanta Men's Soft Toe SRM 3700, Shoe A, Hardness: 52; the DS Work Service 6671, Shoe B, Hardness: 59; Rockport K71224, Shoe C, Hardness: 53) had different outsole materials as well as different tread patterns. The floors (Floors 1–10, see the Supplemental Materials on the ASME Digital Collection for description of flooring and open access to topography data) had varying surface finishes and topography levels. Each shoe and floor combination was analyzed constituting a total of 30 combinations, with nine measurements for each combination, resulting in a total of 270 experimental measurements. The same parameters were used for all model calculations in accordance with experimental testing conditions used within this study and verified values from other literature.

The model parameters $\bar{v}$ and σ_0 were set at 0.5 m/s and 1 MPa respectively, determined by the values used with the slip tester and typical contact pressures relevant to shoe-floor contact [16,17]. A Poisson's ratio υ of 0.499 was used for all calculations, indicating that the material is nearly incompressible [53,54]. To ensure that topography and material-response data were consistent across shoes and flooring, the same limits of integration were used for all shoe and floor simulations. These values were determined by finding the range of wavevectors for each PSD and complex modulus, then selecting limits that were available for all shoe-floor combinations. These limits of integration (q_L to q_1) were $6.28*10^2$ m^{-1} and $2.17*10^8$ m^{-1} corresponding to wavelengths of $1.0*10^{-2}$ m (i.e., 1 cm) and $2.9*10^{-8}$ m respectively (i.e., 29 nm), a range where these techniques are valid [50].

2.2.1 Experimental COF Data Collection. The experimental COF data was collected using the STEPS slip tester (Fig. 1) (XRDS Systems, LLC, Andover, Massachusetts, USA) for each

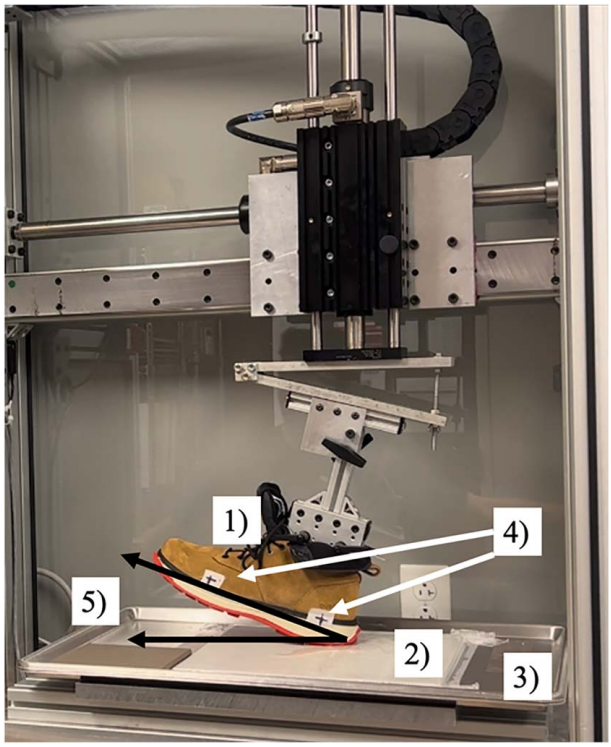

Fig. 1 The slip tester used for experimental data collection of shoe-floor COF with the following components: 1) shoe, 2) floor tile, 3) metal tray for floor attachment, 4) guiding points to measure angle along shoe, and 5) lines denoting shoe-floor angle

shoe-floor combination. Friction tests used a sliding velocity of 0.5 m/s and an applied normal force of 250 N. A digital angle-measurement tool (General Tools, 822 Digital Angle Finder, New York City, New York) was used to ensure the angle between the shoe and floor was 17 deg ± 2 deg. The normal force, shoe-floor angle, and sliding velocity were based on the under-shoe conditions that have been observed when the shoe begins to slip [16,17]. These test methods have been shown to validly predict the onset of slipping [55–57] and are repeatable [58]. These methods have also been adopted as an industry standard (NFSI B101.7) [59]. The COF was the average ratio of shear force to normal force, measured over the 50 ms of sliding after the normal force level was reached [58]. For each trial of COF data collection, canola oil was applied to the floor as a contaminant. This contaminant was selected for its relevance as a real-world contaminant (especially in the restaurant industry) and because it is expected to isolate hysteresis friction [14,22,26,60]. The oil was poured over the contacting region between the shoe and floor until the thickness of the oil in that region did not appear to visually increase with additional fluid. The first three trials that met all force, angle, and velocity requirements were reported. This was repeated on three separate days consisting of nine total COF measurements for each shoe-floor combination. The mean and standard deviation of these measurements were calculated and used for statistical analyses.

2.2.2 Data Collection for the Surface Topography and its Power Spectral Density. Surface topography data was collected for each floor tile using stylus profilometry and SEM. A contact profilometer (DektakXT, Bruker, Billerica, MA) was used at three different locations. Profiles were measured using a 4-mm scan length and point spacing of 0.5 μm. For each floor surface, six line-profile measurements were taken at random orientations (3 locations*6 orientations = 18 total scans). Next, the surfaces were prepared for SEM measurements by cutting them into $1.5 \times 1.5 \times 0.5$ cm^3 samples. These samples were mounted and then polished using standard practices in metallographic sample preparation, so that the cross-sections could be examined. A scanning electron microscope (Sigma 500VP, Zeiss, Oberkochen, Germany) was used to collect ten images in a working distance of less than 1 mm at magnifications of ×5000, ×50,000, and ×100,000 [36]. A PSD for each topography measurement was generated by performing a Fourier transform of the autocorrelation of the height varying with position along the surface. The PSD was calculated following the conventions described in Ref. [35] and all PSD calculations were performed using the CONTACT.ENGINEERING platform [61]. The overall PSD of the surface was found as the average of all PSD curves from the various topography measurements [36,62]. The surface topography used in the Persson model is a two-dimensional (2D) measurement, however the surfaces in this study were characterized as one-dimensional (1D) line scans. Therefore, the 2D PSD was estimated using the 1D data under the assumption that the surface topography was isotropic (Eq. (6)). In this equation, C^{iso} is the 2D PSD measurement, C^{1D} is the 1D measurement, q_x is the current wavevector, and q_s is the maximum wavevector [35]. This process was repeated for all floors, generating one PSD for each surface (Fig. 2).

$$C^{iso}(q_x) \approx \frac{\pi C^{1D}}{q_x}\left(1 - \left(\frac{q_x}{q_s}\right)^2\right)^{-1/2} \tag{6}$$

2.2.3 Measurements of the Dynamic Mechanical Properties of the Shoe Material. The complex (storage and loss) moduli were measured for each shoe material using dynamic mechanical analysis. All testing for this dataset was performed at a commercial testing facility (C-Therm, Fredericton, New Brunswick, Canada). For each shoe, the outsole was separated, and two 10-mm-diameter disc-shaped samples were taken. After being cut and sanded down to a thickness of 2–3 mm, the samples were glued between metal lugs to be loaded into the testing machine (DMA+150, Metravib, Limonest, France). The temperatures ranged from −50 °C to 40 °C, increasing at a rate of 2 °C/min. At each temperature, the sample was sheared using a displacement of 1 μm (2 μm for Shoe C) over a frequency range of 1–200 Hz. The loss and storage moduli were measured at each incrementing temperature over the frequency range. The complex modulus was found as the combination of these two

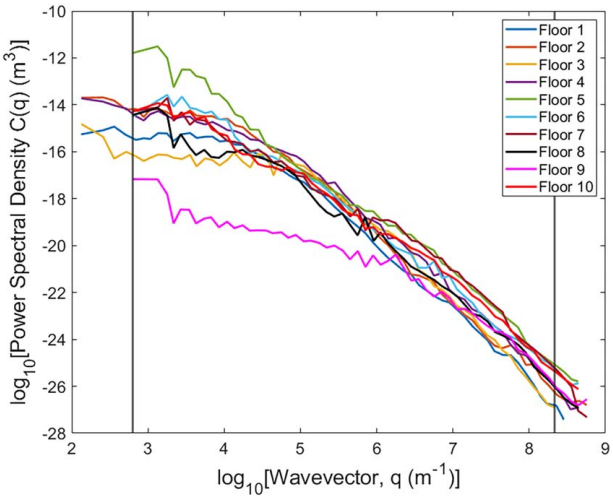

Fig. 2 The topography of all floors is used to compute the 1D power spectral density. The floors were measured using stylus profilometry and SEM. Black vertical lines show the limits of integration used in the full-scale calculations for COF. The identity and topography of each floor type is described in Table S1 available in the Supplemental Materials.

moduli (Eq. (1)). The master curve, accounting for moduli measurements at all desired frequencies, was generated using time-temperature superposition at a reference temperature of 20 °C leading to frequency response with orders of magnitude ranging from 10^{-2} Hz to 10^{8} Hz (Fig. 3).

2.2.4 Statistical Analyses. Accuracy of the model predictions was assessed with a bivariate correlation analysis. The independent variable was the model predictions, and the dependent variable was the experimental values of COF as measured by the slip tester. The determination coefficient R^2 was calculated along with the p value (compared to a Type 1 error rate of $\alpha = 0.05$) and the $\text{RMS}_{\text{error}}$ between the measured COF and the best-fit line. The first correlation analysis, which we call the "full-length-scale implementation of the model", used predictions based on the full range of measured topography, from 10 nm to 1 cm (See vertical lines on Fig. 3). After this initial bivariate correlation analysis, further examination was performed to determine if better correlation could be found using only a limited range of topography, the so-called "limited-length-scale implementation of the model". Model COF results were calculated again using varying upper cutoffs (q_1) between the original limit of integration (Fig. 3, right vertical line) and 10^3 m^{-1}. The value of R^2 was calculated between each new set of predictions and the experimental results. This process was repeated for lower cutoffs (q_L) between the original limit of integration (Fig. 3, left vertical line) and 10^6 m^{-1}. These analyses were performed to test whether disregarding small or large length-scale features improved model predictions. The COF results corresponding to the cutoff yielding the highest R^2 were used to demonstrate improved COF predictions associated with ignoring certain scales of topography.

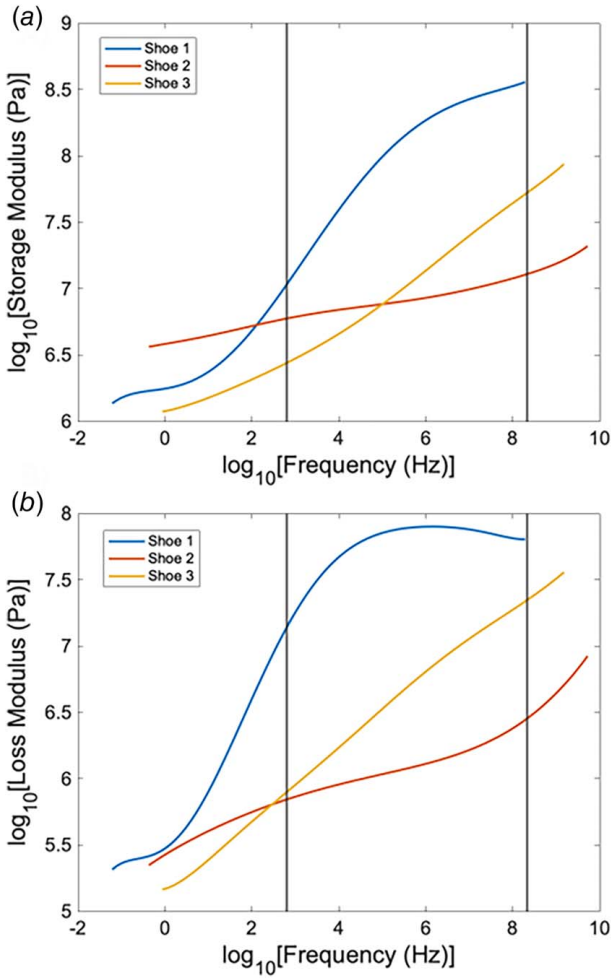

Fig. 3 The (*a*) storage and (*b*) loss moduli for the outsole materials from all shoes is shown as a function of frequency. Vertical lines show the limits of integration that were used for COF model calculations (Eq. (2)). The right vertical line corresponds to the frequency where data was available for all three shoe materials. The left vertical line corresponds to the smallest wavevectors (largest wavelengths) where data was available for all floors given the sliding speeds in this study. The identity and hardness of each shoe is described in the Methods section.

3 Results

3.1 The Full-Length-Scale Implementation of the Model: COF Predictions Using all Available Scales of Topography. The experimentally measured values of COF ranged across an order of magnitude, from 0.052 to 0.54, with a mean of 0.179 and large variability (standard deviation of 0.132). The corresponding predictions of the model, as specified by Eqs. (2)–(4), were significantly higher with a range from 0.272 to 5.524, a mean of 2.050, and a standard deviation of 1.470. While the absolute values were significantly different, an initial bivariate correlation analysis showed a weak yet significant correlation between the experimental and predicted COF values (Fig. 4, $R^2 = 0.168$, $p = 0.024$, RMSE = 0.122).

3.2 The Limited-Length-Scale Implementation of the Model: COF Predictions When a Size Cutoff is Imposed. Because the full-length-scale implementation of the model showed overprediction of COF by approximately an order of magnitude, the model was re-implemented under the assumption that only a limited range of size scales of topography contributed to frictional losses. This limited-length-scale implementation was inspired by prior experimental work indicating that certain size scales contribute more to performance than others [63], although the exact range of scales that matter will vary depending on conditions. In the full-length-scale implementation (prior section), the cutoff values

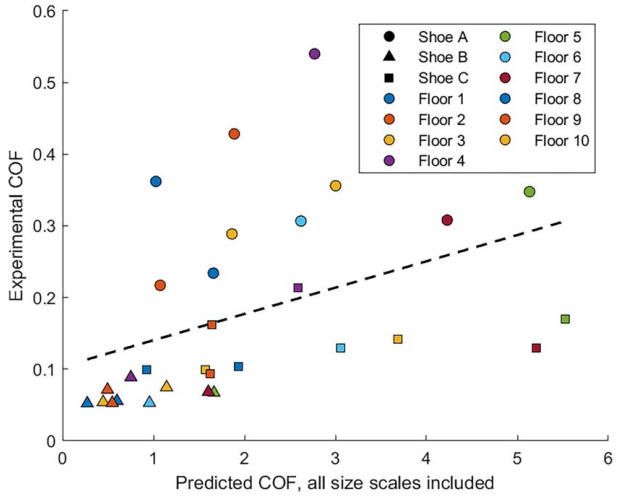

Fig. 4 Using the measured topography across all size scales (full-length-scale implementation), the multiscale mechanics model significantly overpredicted the true values of oily-condition COF. The model prediction with measured results across all measurements has an RMS error (RMSE) of 0.122 (based on the error between measured COF and the best-fit line). However, bivariate correlation between model predictions and experimentally measured results shows a weak, positive correlation. The dotted line shows the regression line for this analysis. Different shoes are denoted by marker shapes whereas different floors are denoted by color. (See main text for identity and properties of all shoes and floors).

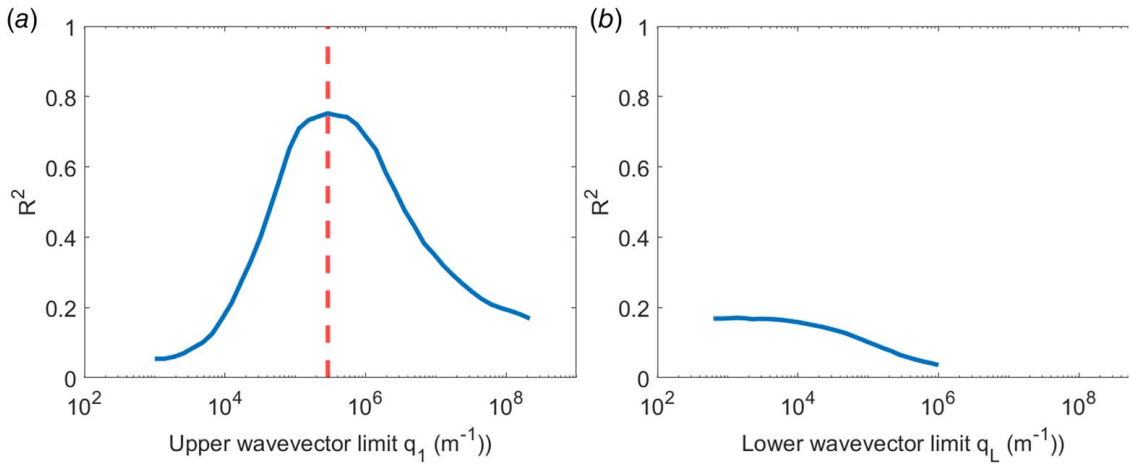

Fig. 5 (*a*) The coefficient of determination is plotted for all cutoff values in the limited-length-scale implementation of the mechanics model. When a small-scale cutoff is imposed, then q_1 is altered (*x*-axis). The dashed vertical line shows the R^2 value is maximized, when a small-scale cutoff is imposed at $q_{1(\text{best-fit})} = 2.91*10^5\ \text{m}^{-1}$, corresponding to a minimum relevant size scale of about 20 microns. (*b*) The coefficient of determination plotted when a large-scale cutoff is imposed, with q_L representing the maximum size scale that was included in computing COF. Since no significant correlation was found at any large wavelength scale cutoff, then the optimal value is not indicated (as it is in panel (*a*)).

were defined by the largest and smallest sizes that could be reliably measured. During the limited-length-scale implementation (this section), COF values were calculated using only a limited range wavevectors, which correspond to a limited range of relevant size scales. These outer values were allowed to vary, since it was not clear *a priori* which ranges of scales would be expected to contribute the most. The limited-length-scale implementation was carried out twice: first with a large-scale cutoff, where q_L was kept constant (set by the smallest scale of measurement) and q_1 was varied; and second with a small-scale cutoff, where $q_1$was kept constant (set by the largest scale of measurement) and q_L was varied. For each value of cutoff during both runs, the R^2 was calculated between experiments and simulations, with results shown in Fig. 5.

Modifying the small-scale cutoff vastly improved the correlation (Fig. 5(*a*)); whereas modifying the large-scale cutoff did not (R^2 values were below 0.17, as shown in Fig. 5(*b*), and therefore it is considered to be a poor fit to the data regardless of the chosen value of q_L). The greatest R^2 value corresponded to an upper q limit of integration of $2.91*10^5\ \text{m}^{-1}$; however, there was a range of cutoff values from approximately $1*10^5\ \text{m}^{-1}$ to $1*10^6\ \text{m}^{-1}$ where the R^2 was greater than 0.6. The optimal upper wavevector cutoff corresponded to an asperity wavelength of 21.6 μm, with wavevectors greater than the cutoff corresponding to smaller wavelengths. The model calculations with this upper q cutoff (q_1) of $2.91*10^5\ \text{m}^{-1}$ had a mean and standard deviation of 0.415 and 0.401 respectively with a range from 0.001 to 1.555. The absolute values of the predictions were still approximately twice as large as experimental values; however, the bivariate correlation analysis using these COF predictions (Fig. 6) corresponded to an R^2 value of 0.752 with $p < 0.0001$ and an $\text{RMS}_{\text{error}}$ of 0.066. In summary, the exclusion of small-scale features from the model did improve the correlation between model results and experimentally measured COF, but the exclusion of large-scale features did not improve the correlation.

4 Discussion

The full-length-scale implementation of the model was somewhat predictive of friction ($p = 0.024$, $\text{RMS}_{\text{error}} = 0.122$ calculated based on the fit line) but predictions improved significantly in the limited-length-scale implementation, when excluding small-scale topography beyond a wavevector of $2.91*10^5\ \text{m}^{-1}$ ($p < 0.0001$, $\text{RMS}_{\text{error}} = 0.066$), corresponding to a size of 21.6 microns. The predictive performance of the model got worse when excluding large-scale topography features. In both the full-length-scale implementation and the limited-length-scale implementation, the predicted COF values were higher than those observed experimentally. However, the model predictions were within an order of magnitude of the experimentally measured values when excluding the small-scale features.

4.1 Lubrication Mechanism May Explain Better Model Performance When Small-Scale Features Were Omitted. The improvement of the model when removing the small-scale features may provide insights into the lubrication mechanism and how it affects the contribution of different topography scales. The model did not consider hydrodynamic effects of the fluid and instead only assumes that the fluid eliminates adhesion

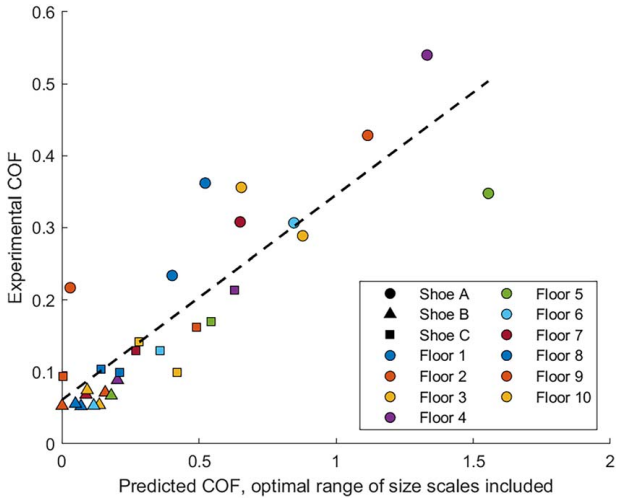

Fig. 6 Bivariate correlation between the limited-length-scale implementation of the COF model and experimentally measured results, with the optimal upper cutoff to the limit of integration of $q = 2.91*10^5\ \text{m}^{-1}$. The dashed line shows the trendline for the analysis. Different shoes are denoted by marker shapes whereas different floors are denoted by color; see main text for identity and properties of all shoes and floors.

friction. Although prior research has indicated that fluid pressures (measured with fluid pressure sensors) are only present when worn shoes or large tread features are combined with high-viscosity fluids, predictions of film thickness indicate that small film thicknesses can form for all shoes [64,65]. These small film thicknesses may influence small-scale contact but without being measured by fluid pressure sensors (with inlets of ~1 mm) and may not impact the contact of large-scale features [7,11,64]. These potential outcomes are consistent with arguments from prior researchers that liquid contaminants effectively reduce the topography of smaller-size-scale asperities (i.e., acting like a low-wavevector-pass filter) while larger asperities remained unaffected [25,66]. Another potential mechanism for why small-scale features may not have contributed to friction is the potential for fluid contaminants to become trapped in wells within the apparent contact region and then sealed in by the surface asperities [25,66,67]. There may be a scale dependence of the formation of these sealed regions that differently affects topography at different scales. For example, sealed regions of fluid are unlikely to influence floor asperities if the size of the sealed region is smaller than the scale of an asperity.

The predicted COF values, even after the small-scale features were ignored by the model, were substantially higher than the experimentally measured values. This suggests that the model is still overpredicting shoe-floor coefficient of friction potentially due to underestimating the full impact of the fluid. One potential reason for the underestimation arises from our implementation of a hard cutoff at certain scales. This implicitly assumes that there is a binary cutoff, where topography at scales of 25 microns contributes fully (as predicted by the model) and topography at scales of 20 microns contributes not at all. Future research will explore the effect of a more gradual cutoff, or other numerical implementations that may more accurately reflect the physics of the fluid. This may explain why the predicted values were consistently higher than the experimentally measured values. Incorporating the scale-dependent lubricating effect of fluid may lead to predicted values more in line with those measured experimentally.

4.2 Contextualizing the Model: Performance Relative to Other Models, Use Cases, and Scope of Validity. The model tested in this study offers similar predictive ability to other shoe-floor friction models but, unlike statistical models based on roughness parameters, is far more likely to provide validity across different circumstances. Prior research from some of the present authors has developed a multiscale finite element model [30] and statistical model [14,68] (based on tread surface area, hardness, and heel shape) that led to an RMS error of 0.11 (not reported in the study but calculated based on the data) and 0.05, respectively. These two models were primarily focused on geometric features of footwear and each only included 2 flooring samples. The RMS error observed for the present study with small-scale features excluded was 0.07, which was in line with these prior studies. Although this model demonstrated a somewhat lower RMS error than other models that have been presented in the literature, future research is needed to perform head-to-head comparisons across these different modeling approaches using the same data sets.

Beyond the predictive ability, the present model has other advantages given that it is designed to capture the effects of shoe material properties and multiscale floor topography. The present study demonstrated a good ability to differentiate across three shoe materials and across a larger sample of flooring. Another advantage of the present model over the finite element models is that it is computationally more efficient and does not require the same level of expertise as finite element modeling. While coding the model reported by Persson requires expertise in numerical integration techniques, the implementation of this model (once the code has been developed) does not require a high degree of specialized training. Finite element modeling, on the other hand, requires extensive expertise to implement, including meshing, the establishment of boundary conditions, material selection, and contact formulation. Thus, the present model (when excluding small-scale features) offers similar predictive ability but requires less expertise than finite element modeling and may be better positioned to capture material and floor topography effects on friction. Finally, the current study utilized both physics- and data-driven approaches by creating a regression model that utilized friction predictions from the physics-based model. This regression model was needed since the predicted friction values were substantially higher than the experimentally measured values. The previously developed finite element model also utilized both physics and statistics by applying a regression equation to the predicted values. In that finite element model, the predicted friction values were substantially lower than the experimentally measured values. Thus, the need to use both statistics and physics for the prediction model is consistent with prior modeling approaches [30]. One limitation with the use of statistics-based methods is the potential for overfitting. Thus, subsequent validation analyses should be performed to determine if the same fit equation is applicable when considering other data sets.

This study informs three potential use cases for the utilized viscoelastic hysteresis model. First, it may be useful in predicting the impact of shoe material on shoe friction performance in oily or other slippery conditions where hysteresis friction dominates. In particular, the model may be effective at screening a library of materials with known DMA results against a range of flooring. This opportunity is especially interesting as the library of floor topography characterization grows (for example, through the CONTACT.ENGINEERING web application and FAIR data repository [61]). Second, the model may be useful in determining how changes to flooring (e.g., through roughening a particular scale) would influence friction. A library of DMA data is emerging for different shoe materials including in the current study [69] as well as other recent studies [70]. Third, it may eventually be possible for safety professionals to apply the model to select combinations of footwear and flooring that optimize friction performance in slippery environments. Such a process would require broad access to the model, widely available spectral properties of flooring, and material data of footwear.

The validation performed in this study was better positioned to assess the impact of flooring topography on shoe-floor friction as opposed to shoe design given the limited number of shoes (3) and lack of systematic control across their design parameters (material, tread design). Thus, the validity of the model for predicting oily friction when omitting small topography features should be interpreted as being applicable to predicting the impact of topography on oily friction for hard-floor materials. The fact that this relationship held across three shoes provides some confidence that the model is generalizable beyond a single shoe design. However, further validation of the model should be conducted across shoes with controlled tread geometry but different material properties. Lastly, the shoe materials had different time-dependent material properties for both the storage and the loss modulus. We would expect that an increase in storage modulus (assuming that the loss modulus remained constant) would lead to a reduction in the real area of contact ($P(q)$) and thus reduce the predicted coefficient of friction. Furthermore, an increase in loss modulus (when the storage modulus remains constant) would increase friction due to its presence in the numerator of Eq. (2). Future studies that perform a sensitivity analysis to this model by systematically varying these properties would advance the understanding of the friction response to these inputs.

4.3 Limitations and Conclusions. There were limitations with this study, both in experimental setup and characterizing the model. Shoe geometries, specifically outsole tread patterns, impact friction yet these effects were not included in the model [71,72]. The model best predicted oily friction when small-scale features were excluded. This effect was explained by potential hydrodynamic or sealing effects yet future experimental analyses would be needed to confirm the mechanism behind this finding.

Extending this study to a wider range of footwear is needed to get a more robust estimate of the model's validity across footwear.

In conclusion, this study showed that the viscoelastic hysteresis model presented by Persson [25] was able to significantly predict oily shoe-floor friction when multiscale topography was included and smallest-scale floor surface asperities were excluded. The contaminant may have "filtered" these scales either due to hydrodynamic effects or fluid-sealing effects. Compared to finite element analysis or statistical models currently used to predict shoe-floor friction, this model has similar accuracy but is expected to better capture shoe-material and floor-topography effects and can be performed faster and with less expertise than finite element analysis. Footwear, flooring, and safety professionals may benefit from using this model to create safer products and workplaces.

Acknowledgment

Author Kurt Beschorner would like to first thank Dr. Michael Lovell who inspired the quest to identify a multiscale mechanics model that predicts shoe-floor friction. He remembers Dr. Lovell as a tremendous scientist, mentor, and friend. The authors are honored to contribute this study, a result from his inspiration, to this special issue in his memory.

This research was funded by the National Institute for Occupational Safety and Health (R21OH012126). The authors would like to thank Lars Pastewka for providing technical assistance in processing surface topography data. The team would further like to thank Mark Redfern for providing feedback on the model. Finally, the team would like to thank Travis Parkman and C-Therm for their assistance in characterizing footwear materials.

Conflict of Interest

There are no conflicts of interest.

Data Availability Statement

The data and information that support the paper are freely available.[2]

Nomenclature

$A(\lambda)$ = apparent area of contact
$A(L)$ = nominal area of contact
$C(q)$ = power spectral density
C^{iso} = 2-dimensional power spectral density of floor topography
C^{1D} = 1-dimensional power spectral density of floor topography
COF = coefficient of friction
E = elastic modulus
E' = complex modulus
E'' = loss modulus
$G(q)$ = coefficient incorporating topography, material properties, speed, and pressure
$P(q)$ = ratio of A(λ) to A(L)
q = wavevector
q_1 = largest wavevector
q_L = smallest wavevector
q_x = current wavevector
q_s = maximum wavevector
$\bar{v}$ = sliding velocity
λ = wavelength
λ_1 = smallest wavelength
λ_L = largest wavelength
ν = Poisson's ratio
σ_0 = normal pressure
ϕ = angle between the sliding direction and the slope direction
ω = angular frequence ($\omega = 2\pi\bar{v}/\lambda$)

[2]http://dx.doi.org/10.18117/sprd-fm64, Ref. [69].

References

[1] 2022, Numbers of Nonfatal Occupational Injuries and Illnesses by Industry and Case Types, https://www.bls.gov/iif/nonfatal-injuries-and-illnesses-tables/table-2-injury-and-illness-counts-by-industry-2022-national.htm
[2] 2021, Fatal Occupational Injuries by Occupation and Event or Exposure, All United States, https://www.bls.gov/iif/fatal-injuries-tables/fatal-occupational-injuries-table-a-5-2021.htm
[3] Courtney, T. K., Sorock, G. S., Manning, D. P., Collins, J. W., and Holbein-Jenny, M. A., 2001, "Occupational Slip, Trip, and Fall-Related Injuries can the Contribution of Slipperiness be Isolated?," Ergonomics, **44**(13), pp. 1118–1137.
[4] 2023, 2023 Workplace Safety Index, https://business.libertymutual.com/insights/2023-workplace-safety-index/
[5] Redfern, M. S., Cham, R., Gielo-Perczak, K., Grönqvist, R., Hirvonen, M., Lanshammar, H., Marpet, M., Pai IV, C. Y.-C., and Powers, C., 2001, "Biomechanics of Slips," Ergonomics, **44**(13), pp. 1138–1166.
[6] Strandberg, L., and Lanshammar, H., 1981, "The Dynamics of Slipping Accidents," J. Occup. Accid., **3**(3), pp. 153–162.
[7] Chang, W.-R., Grönqvist, R., Leclercq, S., Myung, R., Makkonen, L., Strandberg, L., Brungraber, R. J., Mattke, U., and Thorpe, S. C., 2001, "The Role of Friction in the Measurement of Slipperiness, Part 1: Friction Mechanisms and Definition of Test Conditions," Ergonomics, **44**(13), pp. 1217–1232.
[8] Chang, W.-R., Grönqvist, R., Leclercq, S., Brungraber, R. J., Mattke, U., Strandberg, L., Thorpe, S. C., Myung, R., Makkonen, L., and Courtney, T. K., 2001, "The Role of Friction in the Measurement of Slipperiness, Part 2: Survey of Friction Measurement Devices," Ergonomics, **44**(13), pp. 1233–1261.
[9] Beschorner, K. E., Albert, D. L., and Redfern, M. S., 2016, "Required Coefficient of Friction During Level Walking is Predictive of Slipping," Gait Posture, **48**, pp. 256–260.
[10] Hanson, J. P., Redfern, M. S., and Mazumdar, M., 1999, "Predicting Slips and Falls Considering Required and Available Friction," Ergonomics, **42**(12), pp. 1619–1633.
[11] Beschorner, K. E., Redfern, M. S., Porter, W. L., and Debski, R. E., 2007, "Effects of Slip Testing Parameters on Measured Coefficient of Friction," Appl. Ergon., **38**(6), pp. 773–780.
[12] Blanchette, M. G., and Powers, C. M., 2015, "Slip Prediction Accuracy and Bias of the SATRA STM 603 Whole Shoe Tester," J. Test. Eval., **43**(3), pp. 491–498.
[13] Blanchette, M. G., and Powers, C. M., 2015, "The Influence of Footwear Tread Groove Parameters on Available Friction," Appl. Ergon., **50**, pp. 237–241.
[14] Iraqi, A., Vidic, N. S., Redfern, M. S., and Beschorner, K. E., 2020, "Prediction of Coefficient of Friction Based on Footwear Outsole Features," Appl. Ergon., **82**, p. 102963.
[15] Jones, T., Iraqi, A., and Beschorner, K., 2018, "Performance Testing of Work Shoes Labeled as Slip Resistant," Appl. Ergon., **68**, pp. 304–312.
[16] Albert, D., Moyer, B., and Beschorner, K. E., 2017, "Three-Dimensional Shoe Kinematics During Unexpected Slips: Implications for Shoe–Floor Friction Testing," IISE Trans. Occup. Ergon. Hum. Factors, **5**(1), pp. 1–11.
[17] Iraqi, A., Cham, R., Redfern, M. S., Vidic, N. S., and Beschorner, K. E., 2018, "Kinematics and Kinetics of the Shoe During Human Slips," J. Biomech., **74**, pp. 57–63.
[18] Bell, J. L., Collins, J. W., and Chiou, S., 2019, "Effectiveness of a no-Cost-to-Workers, Slip-Resistant Footwear Program for Reducing Slipping-Related Injuries in Food Service Workers," Scand. J. Work, Environ. Health, **45**(2), pp. 194–202.
[19] Cockayne, S., Fairhurst, C., Frost, G., Liddle, M., Cunningham-Burley, R., Zand, M., Hewitt, C., Iles-Smith, H. M., Green, L., and Torgerson, D. J., 2021, "Slip-Resistant Footwear Reduces Slips Among National Health Service Workers in England: a Randomised Controlled Trial," Occupat. Environ. Med., **78**(7), pp. 472–478.
[20] Verma, S. K., Chang, W. R., Courtney, T. K., Lombardi, D. A., Huang, Y.-H., Brennan, M. J., Mittleman, M. A., Ware, J. H., and Perry, M. J., 2011, "A Prospective Study of Floor Surface, Shoes, Floor Cleaning and Slipping in US Limited-Service Restaurant Workers," Occupat. Environ. Med., **68**(4), pp. 279–285.
[21] Verma, S. K., Zhao, Z., Courtney, T. K., Chang, W.-R., Lombardi, D. A., Huang, Y.-H., Brennan, M. J., and Perry, M. J., 2014, "Duration of Slip-Resistant Shoe Usage and the Rate of Slipping in Limited-Service Restaurants: Results From a Prospective and Crossover Study," Ergonomics, **57**(12), pp. 1919–1926.
[22] Cowap, M. J., Moghaddam, S. R., Menezes, P. L., and Beschorner, K. E., 2015, "Contributions of Adhesion and Hysteresis to Coefficient of Friction Between Shoe and Floor Surfaces: Effects of Floor Roughness and Sliding Speed," Tribol. Mater., Surf. Interfaces, **9**(2), pp. 77–84.
[23] Mate, C. M., and Carpick, R. W., 2019, *Tribology on the Small Scale: A Modern Textbook on Friction, Lubrication, and Wear*, Oxford University Press, Oxford, UK.
[24] Moore, C. T., Menezes, P. L., Lovell, M. R., and Beschorner, K. E., 2012, "Analysis of Shoe Friction During Sliding Against Floor Material: Role of Fluid Contaminant," ASME J. Tribol., **134**(4), p. 041104.
[25] Persson, B. N., 2001, "Theory of Rubber Friction and Contact Mechanics," J. Chem. Phys., **115**(8), pp. 3840–3861.
[26] Strobel, C. M., Menezes, P. L., Lovell, M. R., and Beschorner, K. E., 2012, "Analysis of the Contribution of Adhesion and Hysteresis to Shoe–Floor Lubricated Friction in the Boundary Lubrication Regime," Tribol. Lett., **47**(3), pp. 341–347.
[27] Cowap, M., and Beschorner, K., 2012, "The Effects of Floor Roughness on Shoe-Floor Friction Adhesion and Hysteresis," International Joint Tribology Conference, Denver, CO, Oct. 7–10, pp. 111–113.

[28] Hardy, W. B., and Bircumshaw, I., 1925, "Bakerian Lecture.-Boundary Lubrication.-Plane Surfaces and the Limitations of Amontons' Law," Proc. R. Soc. London, Ser. A, Containing Papers Math. Phys. Charact., **108**(745), pp. 1–27.
[29] Israelachvili, J. N., 2005, "Importance of Pico-Scale Topography of Surfaces for Adhesion, Friction, and Failure," MRS Bulletin, **30**(7), pp. 533–539.
[30] Moghaddam, S. R., Acharya, A., Redfern, M. S., and Beschorner, K. E., 2018, "Predictive Multiscale Computational Model of Shoe-Floor Coefficient of Friction," J. Biomech., **66**, pp. 145–152.
[31] Chang, W.-R., 1998, "The Effect of Surface Roughness on Dynamic Friction Between Neolite and Quarry Tile," Safety Sci., **29**(2), pp. 89–105.
[32] Randolph, A. B., Reifler, K., Chadha, V., Jacobs, T. D., and Beschorner, K. E., 2024, "The Need for Better Metrics for Floor-Tile Topography: Conventional Metrics Correlate Only Modestly with Shoe-Floor Friction," Tribol. Int., **193**, p. 109366.
[33] Chang, W.-R., Grönqvist, R., Hirvonen, M., and Matz, S., 2004, "The Effect of Surface Waviness on Friction Between Neolite and Quarry Tiles," Ergonomics, **47**(8), pp. 890–906.
[34] Chang, W.-R., Matz, S., Grönqvist, R., and Hirvonen, M., 2010, "Linear Regression Models of Floor Surface Parameters on Friction Between Neolite and Quarry Tiles," Appl. Ergon., **41**(1), pp. 27–33.
[35] Jacobs, T. D., Junge, T., and Pastewka, L., 2017, "Quantitative Characterization of Surface Topography Using Spectral Analysis," Surf. Topogr. Metrol. Prop., **5**(1), p. 013001.
[36] Ding, R., Gujrati, A., Pendolino, M. M., Beschorner, K. E., and Jacobs, T. D., 2021, "Going Beyond Traditional Roughness Metrics for Floor Tiles: Measuring Topography Down to the Nanoscale," Tribol. Lett., **69**(3), p. 92.
[37] Borodich, F. M., Pepelyshev, A., and Jin, X., 2024, "A Multiscale Statistical Analysis of Rough Surfaces and Applications to Tribology," Mathematics, **12**(12), p. 1804.
[38] Sokoloff, J., 2012, "Surface Roughness and Dry Friction," Phys. Rev. E: Stat., Nonlinear, Soft Matter Phys., **85**(2), p. 027102.
[39] Henriques, I., Borges, L., Costa, M., Soares, B., and Castello, D., 2018, "Comparisons of Complex Modulus Provided by Different DMA," Polym. Test., **72**, pp. 394–406.
[40] Cowie, J. M. G., and Arrighi, V., 2007, *Polymers: Chemistry and Physics of Modern Materials*, CRC Press, Boca Raton, FL.
[41] Artiaga, R., and García-Diez, A., 2005, *Fundamentals of DMA*, Departamento de Ingeniería Industrial II. Escola Politécnica Superior, Universidade da Coruña.
[42] Chartoff, R. P., Menczel, J. D., and Dillman, S. H., 2009, *Thermal Analysis of Polymers: Fundamentals and Applications*, Wiley, Hoboken, NJ, pp. 387–495.
[43] Campañá, C., and Müser, M. H., 2007, "Contact Mechanics of Real vs. Randomly Rough Surfaces: A Green's Function Molecular Dynamics Study," Europhys. Lett., **77**(3), p. 38005.
[44] Dalvi, S., Gujrati, A., Khanal, S. R., Pastewka, L., Dhinojwala, A., and Jacobs, T. D., 2019, "Linking Energy Loss in Soft Adhesion to Surface Roughness," Proc. Natl. Acad. Sci. USA, **116**(51), pp. 25484–25490.
[45] Kabir, M., Lovell, M. R., and Higgs, C. F., 2008, "Utilizing the Explicit Finite Element Method for Studying Granular Flows," Tribol. Lett., **29**(2), pp. 85–94.
[46] Lovell, M. R., 2001, "Evaluation of Critical Interfacial Friction in Cross Wedge Rolling," ASME J. Tribol., **123**(2), pp. 424–429.
[47] Hale, J., O'Connell, A., Lewis, R., Carré, M., and Rongong, J., 2021, "An Evaluation of Shoe Tread Parameters Using FEM," Tribol. Int., **153**, p. 106570.
[48] Heinrich, G., Klüppel, M., and Vilgis, T. A., 2000, "Evaluation of Self-Affine Surfaces and Their Implication for Frictional Dynamics as Illustrated with a Rouse Material," Comput. Theor. Polym. Sci., **10**(1-2), pp. 53–61.
[49] Jakobsen, L., 2023, *Elastomer Friction–Fundamental and Footwear Research*, Technical University of Denmark, Lyngby, Denmark.
[50] Chadha, V., Miller, N., Ding, R., Beschorner, K. E., and Jacobs, T. D., 2024, "Evaluating Scanning Electron Microscopy for the Measurement of Small-Scale Topography," Surf. Topogr.: Metrol. Prop., **12**(3), p. 035010.
[51] Liu, Y., and Glass, G., 2013, "Effects of mesh density on finite element analysis," No. 0148-7191, SAE Technical Paper.
[52] Ing, H., 2024, "Prediction of Oily Shoe-Floor Friction Using a Multiscale Hysteresis Mechanics Model," Unpublished Master's Thesis, University of Pittsburgh, Pittsburgh, PA.
[53] Centeno Gil, O. J., 2009, Finite Element Modeling of Rubber Bushing for Crash Simulation-Experimental Tests and Validation.
[54] Suh, J. B., 2007, *Stress Analysis of Rubber Blocks Under Vertical Loading and Shear Loading*, University of Akron, Akron, OH.
[55] Beschorner, K. E., Chanda, A., Moyer, B. E., Reasinger, A., Griffin, S. C., and Johnston, I. M., 2023, "Validating the Ability of a Portable Shoe-Floor Friction Testing Device, NextSTEPS, to Predict Human Slips," Appl. Ergon., **106**, p. 103854.
[56] Iraqi, A., Cham, R., Redfern, M. S., and Beschorner, K. E., 2018, "Coefficient of Friction Testing Parameters Influence the Prediction of Human Slips," Appl. Ergon., **70**, pp. 118–126.
[57] Sundaram, V., Hemler, S. L., Chanda, A., Haight, J. M., Redfern, M. S., and Beschorner, K. E., 2020, "Worn Region Size of Shoe Soles Impacts Human Slips: Testing a Mechanistic Model," J. Biomech., p. 109797.
[58] Beschorner, K. E., Iraqi, A., Redfern, M. S., Moyer, B. E., and Cham, R., 2020, "Influence of Averaging Time-Interval on Shoe-Floor-Contaminant Available Coefficient of Friction Measurements," Appl. Ergon., **82**, p. 102959.
[59] NFSI, 2021, *NFSI B101.7: Standard Test Method for Lab Measurement of Footwear Heel Outsole Material Slip Resistance on Liquid-Contaminated Floor Surfaces*, The National Floor Safety Institute, Southlake, TX.
[60] Moghaddam, S. R. M., Redfern, M. S., and Beschorner, K. E., 2015, "A Microscopic Finite Element Model of Shoe–Floor Hysteresis and Adhesion Friction," Tribol. Lett., **59**(1), pp. 1–10.
[61] Röttger, M. C., Sanner, A., Thimons, L. A., Junge, T., Gujrati, A., Monti, J. M., Nöhring, W. G., Jacobs, T. D., and Pastewka, L., 2022, "Contact. Engineering—Create, Analyze and Publish Digital Surface Twins From Topography Measurements Across Many Scales," Surf. Topogr. Metrol. Prop., **10**(3), p. 035032.
[62] Gujrati, A., Khanal, S. R., Pastewka, L., and Jacobs, T. D., 2018, "Combining TEM, AFM, and Profilometry for Quantitative Topography Characterization Across all Scales," ACS Appl. Mater. Interfaces, **10**(34), pp. 29169–29178.
[63] Thimons, L. A., Gujrati, A., Sanner, A., Pastewka, L., and Jacobs, T. D., 2021, "Hard-Material Adhesion: Which Scales of Roughness Matter?," Exp. Mech., **61**(7), pp. 1109–1120.
[64] Hemler, S. L., Charbonneau, D. N., and Beschorner, K. E., 2020, "Predicting Hydrodynamic Conditions Under Worn Shoes Using the Tapered-Wedge Solution of Reynolds Equation," Tribol. Int., **145**, p. 106161.
[65] Moore, C., and Beschorner, K., "Effect of Shoe Roughness on Shoe-Floor Lubrication," 2010 International Conference on Fall Prevention and Protection, Morgantown, WV, May 2010.
[66] Persson, B. N., Albohr, O., Tartaglino, U., Volokitin, A., and Tosatti, E., 2004, "On the Nature of Surface Roughness with Application to Contact Mechanics, Sealing, Rubber Friction and Adhesion," J. Phys.: Condens. Matter, **17**(1), p. R1–R62.
[67] Kumar, N., Dalvi, S., Sumant, A. V., Pastewka, L., Jacobs, T. D., and Dhinojwala, A., 2024, "Small-Scale Roughness Entraps Water and Controls Underwater Adhesion," Sci. Adv., **10**(32), p. eadn8343.
[68] Beschorner, K. E., Nasarwanji, M., Deschler, C., and Hemler, S. L., 2024, "Prospective Validity Assessment of a Friction Prediction Model Based on Tread Outsole Features of Slip-Resistant Shoes," Appl. Ergon., **114**, p. 104110.
[69] Ing, H., Chadha, V., Jacobs, T. D. B., and Beschorner, K. E., 2025, Data Set for Validation of a Multiscale, Hysteresis Mechanics Model in Predicting Oily Shoe-Floor Friction Across Surfaces With Varying Finishes, University of Pittsburgh, http://dx.doi.org/10.18117/sprd-fm64
[70] Jakobsen, L., Auganaes, S. B., Buene, A. F., Sivebaek, I. M., and Klein-Paste, A., 2023, "Dynamic and Static Friction Measurements of Elastomer Footwear Blocks on ice Surface," Tribol. Int., **178**, p. 108064.
[71] Li, K. W., and Chen, C. J., 2004, "The Effect of Shoe Soling Tread Groove Width on the Coefficient of Friction with Different Sole Materials, Floors, and Contaminants," Appl. Ergon., **35**(6), pp. 499–507.
[72] Li, K. W., Wu, H. H., and Lin, Y.-C., 2006, "The Effect of Shoe Sole Tread Groove Depth on the Friction Coefficient with Different Tread Groove Widths, Floors and Contaminants," Appl. Ergon., **37**(6), pp. 743–748.